

Detecting Privilege Escalation with Temporal Braid Groups

Christophe Parisel*

March 13, 2026

Abstract

Within the Strongly Connected Components (SCCs) formed during the temporal evolution of a Cloud permission graph, we use the Burau Lyapunov exponent LE as an algebraic probe to locate the boundary between two risks regimes and to calibrate cheaper detection instruments. We prove that no Abelian statistic (edge counts, net privilege flow, gate-firing rates) can determine LE; empirically, over 49,972 deployments drawn from a 1000-SCC corpus, temporal braid LE retains partial correlation $r = 0.175$ with deployment structure after controlling for firing rate ($p < 10^{-3}$), while the Abelian counting proxy collapses to $r = 0.001$ ($p = 0.98$): zero residual signal.

The non-commutation advantage is small, but actionable: we show how to leverage it to discriminate the two outstanding risk regimes, that we call dispersed and focused, for automating classification and governing remediation of risky Cloud permission flows.

1 Introduction

The security posture of a cloud identity is not determined by a single permission snapshot but by its full temporal trajectory. Two non-human identities (NHIs) may hold identical permissions today yet diverge tomorrow: one may ratchet irreversibly toward broader access while the other oscillates within a bounded envelope.

In a companion paper [1], we introduced the primorial invariant, which encodes the cycle structure of a Strongly Connected Component (SCC) [5] as a vector of rational numbers and provides a first-pass topological screen: it discriminates *oscillators* (SCCs whose directed edges cannot sustain monotone privilege escalation) from *ratchets* (SCCs with at least one directed WAR path capable of irreversible upward drift). Oscillators are topologically safe and require no further dynamic analysis; ratchets carry escalation potential and must be assessed dynamically.

Within ratchets, a second distinction governs remediation.

A **focused** ratchet concentrates escalation through few paths; non-commutative cancellations moderate spectral growth and WAR reassignment is curative. A **dispersed** ratchet has a hub-rich topology with multiple independent escalation paths; topology surgery (adding or reversing edges) is required.

The central result is that the Burau Lyapunov exponent LE is a small but actionable separator of these two regimes: it is provably beyond the reach of any Abelian statistic (Theorem 6.2). Burau LE serves as both *boundary separator* and *calibration oracle* (validating cheaper instruments). The Abelian gate-firing rate provides a fast first-pass but carries a systematic one-directional bias: it always over-calls dispersed and never the reverse, because it cannot account for non-commutative cancellation.

*Email: ch.parisel@gmail.com

Contributions.

1. **Impossibility result.** No Abelian statistic (edge counts, net privilege flow, or gate-firing rate) can determine LE (Theorem 6.2). A sharp structural instance: any directed cycle in a ratchet SCC contributes exactly zero to DWS for *every* WAR assignment, by a telescoping-sum identity (Theorem 6.3), so directed-cycle topologies have a DWS-invisible escalation channel that the braid walk detects unconditionally. Temporal braid LE retains partial correlation $r = 0.175$ with deployment structure after controlling for firing rate ($p < 10^{-3}$); the Abelian proxy collapses to $r = 0.001$ ($p = 0.98$).
2. **Two-regime classification with Burau as calibration oracle.** LE defines a focused/dispersed boundary that determines which intervention (WAR reassignment vs. topology surgery) is required. Across 49,972 (SCC, WAR) pairs from a 1000-SCC corpus, 5.7% of pairs disagree between Burau and the Abelian rate, with topology-dependent FD/DF structure that the Abelian rate cannot predict.
3. **Gate condition and braid construction.** NHI walkers co-occurring on ascending directed edges inject braid generator $\sigma_i^2 \sigma_{i+1}^{-1}$, coupling graph topology to privilege-flow alignment (Section 3).
4. **Firing-rate lower bound for hub SCCs.** For k -hub SCCs, the firing rate exceeds a topology-derived lower bound (Theorem 4.8); under a spoke-coverage condition the bound places dense hubs unconditionally in the dispersed regime.

2 Background

2.1 Strongly connected components

A *directed graph* $G = (V, E)$ consists of vertices and directed edges. A *strongly connected component* (SCC) is a maximal subgraph in which every vertex is reachable from every other vertex via directed paths. SCCs are the “inescapable neighbourhoods” of a directed graph: once inside, every vertex can reach every other.

In graph theory, determining whether a directed graph is strongly connected is a classical problem (Tarjan’s algorithm runs in linear time). Every directed graph decomposes uniquely into SCCs connected by a directed acyclic graph (DAG) of inter-component edges.

A *cycle* in a directed graph is a closed walk $v_0 \rightarrow v_1 \rightarrow \dots \rightarrow v_k = v_0$. Every SCC with more than one vertex contains at least one cycle; the cycle structure encodes recurrence patterns. When vertices carry scalar labels (in our setting, privilege weights) the label changes along a cycle determine whether the cycle amplifies, dampens, or preserves the scalar quantity.

2.2 Random walks on graphs and Markov chains

A *random walk* on a directed graph $G = (V, E)$ is a discrete Markov chain: from the current vertex v , the walker follows one outgoing edge chosen uniformly at random, reaching neighbour u with probability $P_{vu} = 1/\deg^+(v)$ if $(v, u) \in E$, and $P_{vu} = 0$ otherwise. Here $\deg^+(v)$ is the out-degree of v and $P \in [0, 1]^{|V| \times |V|}$ is the *transition matrix*.

A Markov chain is *irreducible* if every state is reachable from every other state in a finite number of steps. An SCC is precisely the maximal subgraph on which the restricted walk is irreducible: inside an SCC every vertex can reach every other (by strong connectivity), while no edge leaves the component. The random walk confined to an SCC is therefore irreducible by construction.

By the Perron–Frobenius theorem [11], an irreducible aperiodic Markov chain has a unique *stationary distribution* π satisfying $\pi P = \pi$ with $\sum_v \pi(v) = 1$. The stationary mass $\pi(v)$ is

the long-run fraction of time the walker spends at v . For a uniform random walk on a strongly connected graph, $\pi(v)$ is proportional to the in-degree of v : high-fanin vertices accumulate the most visit mass.

In our framework, the NHI walkers of Section 3 perform independent random walks on a fixed ratchet SCC. Irreducibility ensures that the long-run walk statistics are well-defined and independent of starting position. In particular, the Lyapunov exponent (Theorem 4.2) can be consistently estimated from a single trajectory of sufficient length rather than requiring ensemble averages. Stationary mass determines which vertices (hence which edges) are visited most frequently, shaping how often the gate condition fires and which braid generators enter the accumulated product.

2.3 Braid groups

The *braid group* [2] B_n on n strands is the group generated by $\sigma_1, \dots, \sigma_{n-1}$ subject to:

$$\begin{aligned} \sigma_i \sigma_j &= \sigma_j \sigma_i && \text{if } |i - j| \geq 2, && (1) \\ \sigma_i \sigma_{i+1} \sigma_i &= \sigma_{i+1} \sigma_i \sigma_{i+1} && \text{(Yang-Baxter relation).} && (2) \end{aligned}$$

Geometrically, σ_i swaps strands i and $i + 1$ with strand i passing over strand $i + 1$, and σ_i^{-1} is the reverse crossing. A *braid word* is a finite product of generators and their inverses.

2.4 Non-Commutation

A group is *Abelian* (commutative) if $ab = ba$ for all elements. The braid group B_2 is generated by a single element σ_1 and is therefore Abelian. For $n \geq 3$, B_n is *non-Abelian*: $\sigma_1 \sigma_2 \neq \sigma_2 \sigma_1$. This non-commutativity is essential because it allows products of braid generators to exhibit *exponential growth* in matrix representations, the key mechanism underlying our risk metric.

In an Abelian group, matrix representations have eigenvalues on the unit circle and spectral radius 1: no matter how many generators you multiply, the product cannot grow. Non-Abelian words can break this barrier, producing spectral radii strictly greater than 1 and hence exponential growth under iteration.

2.5 The Burau representation

The *Burau representation* is a homomorphism $\rho_t : B_n \rightarrow \text{GL}_n(\mathbb{Z}[t, t^{-1}])$ that sends each braid generator σ_i to an $n \times n$ matrix with entries depending on a formal parameter t . At the specialisation $t = -1$, all entries become integers, enabling exact computation. The spectral radius of the resulting integer matrix product measures how fast the braid “stretches” under iteration. This is the signal we use to quantify risk. Section 4 gives the full definition.

In this framework, the full Burau computation ($N \times N$ matrices, multi-NHI walks) serves as *validation infrastructure*: the non-Abelian ground truth that proves temporal braid LE captures genuine non-Abelian structure beyond the Abelian rate.

3 Construction: Permission Braids with Signal Injection

3.1 Permission transition graphs and the WAR permission scalar

Let $G = (V, E)$ be a directed graph where each vertex $v \in V$ represents a permission state characterised by a scalar, the *WAR norm*[4] $W(v) \in \mathbb{Z}_{\geq 0}$, and each edge $(u, v) \in E$ represents an observed permission transition. Edges are either *directed* ($u \rightarrow v$, irreversible: $v \rightarrow u \notin E$) or *bidirectional* ($u \leftrightarrow v$, reversible: both $u \rightarrow v$ and $v \rightarrow u \in E$).

Definition 3.1 (Directed WAR flow). For an edge $(u \rightarrow v) \in E$, the *WAR flow* is $\delta(u \rightarrow v) = W(v) - W(u)$. A directed edge is *ascending* if $\delta > 0$, *flat* if $\delta = 0$, and *descending* if $\delta < 0$.

3.2 SCC classification

We classify SCCs along two axes:

- **Topology axis:** does the SCC contain at least one directed edge?
- **Privilege axis:** does the current WAR assignment align with the directed edges (ascending flow)?

SCCs with no directed edges are *periodic*: WAR trajectories are mean-reverting, and the braid word produced by walkers on such SCCs is Abelian (all generators commute). These are structurally benign and are fully characterised by the primordial period-2 oscillator class [1].

SCCs with at least one directed edge are *ratchets*. The present paper focuses exclusively on ratchets, since these are the SCCs for which the deployed WAR assignment determines potential severity.

3.3 NHI walkers and strand ordering

Fix a ratchet SCC C with n walkers $\text{NHI}_1, \dots, \text{NHI}_n$ performing simultaneous random walks over $V(C)$. The start positions of each NHI is random, since SCCs do not have a defined entry point (unlike DAGs). At each epoch t , the walkers are ordered by their current WAR values: strand i is assigned to the walker with the i -th smallest WAR value (ties broken by a fixed NHI identifier order).

The simultaneous walker construction is a mathematical device used to generate braid words from a static SCC topology under a given WAR assignment. It does not model real-world concurrency of NHIs, nor does it assume that two identities escalate privileges at the same time in production.

The walkers serve as a sampling mechanism: their concurrent motion induces non-commuting generators capturing structural interactions between directed edges under WAR ordering.

3.4 Gate condition and braid word injection

When two adjacent walkers both step along directed edges in the same epoch, with both edges ascending in privilege, the ratchet has fired: two independent ascending directed edges coexist locally in the WAR-ordered topology. The injected braid word encodes this structural configuration algebraically.

Definition 3.2 (Gate condition). At epoch transition $t \rightarrow t + 1$, the *gate fires* for walkers at ranks i and $i + 1$ if and only if:

1. Both walkers traverse *directed* edges (neither edge is bidirectional), and
2. Both edges have positive net WAR flow: $\delta(\text{edge}_i) > 0$ and $\delta(\text{edge}_{i+1}) > 0$.

The gate fires only when both axes are satisfied at once: the edges must be truly irreversible (directed, not bidirectional), and the privilege flow must run uphill. Either condition alone is insufficient: a directed edge with descending WAR represents a privilege drop, not an escalation.

The gate condition should be understood as an algebraic trigger that enriches the braid word when two ascending directed edges coexist locally in the topology. It is not a claim about synchronized privilege escalation events in operational systems.

Definition 3.3 (Permission braid with word injection). The *permission braid* $\beta_C \in B_n$ is an algebraic probe of SCC potential severity. It is constructed as follows. At each epoch $t \rightarrow t + 1$, for each adjacent pair of walkers at ranks i and $i + 1$:

1. If the gate fires (Theorem 3.2): append $\sigma_i^2 \sigma_{i+1}^{-1}$ to the braid word.
2. Otherwise: append nothing (the pair contributes no generators at this step).

Rank swaps that do not satisfy the gate condition are deliberately excluded. A lone generator $\sigma_i^{\pm 1}$ has Burau eigenvalues on the unit circle (SR = 1 at $t = -1$), so it contributes no spectral growth. Including such generators would increase the matrix product length without adding signal.

3.5 The injection word

The injection word must have spectral radius > 1 under the Burau representation at $t = -1$, so that repeated gate firings drive exponential growth of the accumulated matrix product.

Any word with SR > 1 must involve at least two *adjacent* generator indices: single-index words stay Abelian (SR = 1), and non-adjacent generators commute (SR = 1). The shortest candidate is $\sigma_i \sigma_{i+1}^{-1}$ (length 2, SR = $\phi^2 \approx 2.618$), but many non-Abelian words of length 3 also qualify. Among them, we select $\sigma_i^2 \sigma_{i+1}^{-1}$ for its higher spectral radius: SR = $2 + \sqrt{3} \approx 3.732$, a $1.43\times$ lift over the length-2 word (Theorem 3.4).

Adjacent-position cancellation. All words of the form $\sigma_i^a \sigma_{i+1}^b$ with opposite-sign exponents share a structural limitation: when two such words fire at adjacent positions i and $i + 1$ within the same epoch, the inner generators cancel algebraically at least partially, reducing the spectral radius. For our word: $\sigma_i^2 \sigma_{i+1}^{-1} \cdot \sigma_{i+1}^2 \sigma_{i+2}^{-1} = \sigma_i^2 \sigma_{i+1} \sigma_{i+2}^{-1}$, with SR reduced to 1 (the Burau matrix of this word has finite order 6 in $\text{GL}(3, \mathbb{Z})$, so all its eigenvalues are roots of unity). The same holds for the length-2 alternative: $\sigma_i \sigma_{i+1}^{-1} \cdot \sigma_{i+1} \sigma_{i+2}^{-1} = \sigma_i \sigma_{i+2}^{-1}$, also yielding SR = 1 (non-adjacent generators commute and are individually unipotent at $t = -1$, so their product is unipotent).

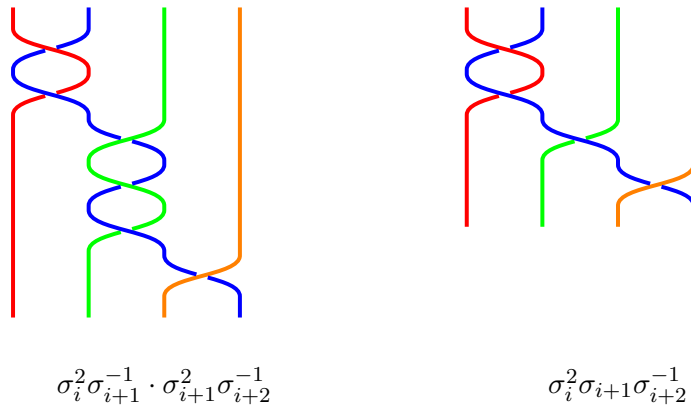


Figure 1: Adjacent-position cancellation: $\sigma_i^2 \sigma_{i+1}^{-1} \cdot \sigma_{i+1}^2 \sigma_{i+2}^{-1}$ collapses to a Burau-flat braid with spectral radius 1.

The adjacent-pair guard (Section 3.4) prevents this within-epoch cancellation by skipping position $i + 1$ whenever position i fires. Cross-epoch interactions at adjacent positions are not cancelled algebraically: they compose non-trivially, producing the spectral cancellation that the shuffling experiment detects (Section 5.2).

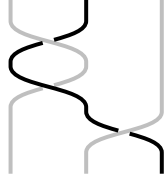


Figure 2: The injection word $\sigma_1^2 \sigma_2^{-1}$ on three strands. Two positive crossings of strands 1–2 followed by one negative crossing of strands 2–3 produce a genuinely non-Abelian braid with $\text{SR} = 2 + \sqrt{3}$.

Each time the gate fires, the injection word’s Burau matrix is multiplied into the running product. The dominant eigenvalue governs the per-injection growth factor of that product: if it exceeds 1, the spectral radius of the accumulated matrix grows exponentially in the number of gate firings, producing a positive Lyapunov exponent. A dominant eigenvalue of exactly 1 would mean no growth at all (the braid is “flat”). The further above 1, the faster the braid stretches under iteration, and the stronger the risk signal.

Proposition 3.4 (Spectral radius of the injection word). *The Burau matrix at $t = -1$ of $\sigma_i^2 \sigma_{i+1}^{-1}$ has characteristic polynomial with roots $\{1, 2 + \sqrt{3}, 2 - \sqrt{3}\}$. The dominant eigenvalue is $2 + \sqrt{3} \approx 3.732$.*

Proof sketch. Working in the unreduced Burau representation at $t = -1$, the active 2×2 block of each generator is

$$\rho_{-1}(\sigma_i)|_{(i, i+1)} = \begin{pmatrix} 2 & -1 \\ 1 & 0 \end{pmatrix},$$

with identity on all other strands. Squaring gives

$$\rho_{-1}(\sigma_i^2)|_{(i, i+1)} = \begin{pmatrix} 2 & -1 \\ 1 & 0 \end{pmatrix}^2 = \begin{pmatrix} 3 & -2 \\ 2 & -1 \end{pmatrix}.$$

Since $\det \rho_{-1}(\sigma_j) = 1$ for all j , the inverse block is $\rho_{-1}(\sigma_{i+1}^{-1})|_{(i+1, i+2)} = \begin{pmatrix} 0 & 1 \\ -1 & 2 \end{pmatrix}$. Evaluating the product explicitly for $n = 3$ strands yields a 3×3 matrix with characteristic polynomial $(\lambda - 1)(\lambda^2 - 4\lambda + 1) = 0$, giving roots 1 and $\lambda = 2 \pm \sqrt{3}$. \square

3.6 Braid word length tradeoffs

Beyond shorter length-2 words which slightly reduce complexity, a natural alternative is a positive-only length-3 word such as $\sigma_i^2 \sigma_{i+1}$ or $\sigma_i \sigma_{i+1} \sigma_i$. Both have $\text{SR} > 1$ and would formally satisfy the growth requirement. However, the mixed-sign choice $\sigma_i^2 \sigma_{i+1}^{-1}$ is load-bearing in two distinct ways that positive-only words cannot replicate.

Cross-epoch cancellations. The negative exponent σ_{i+1}^{-1} creates the possibility that the trailing generator of one gate firing partially cancels the leading generator of the next when they occur at adjacent positions in consecutive epochs. A positive-only injection word makes concatenation strictly length-monotone: every firing lengthens the accumulated word, so word length alone is a reliable proxy for risk. Abelian statistics (DWS, counting-LE, raw firing rate) then track growth faithfully, and the non-Abelian correction supplied by Burau is marginal. The mixed-sign word reintroduces cross-epoch cancellations that Abelian statistics are blind to, making Burau’s signal genuinely irreplaceable.

Signed interference and spectral resonance. The high spectral radius $2 + \sqrt{3}$ arises from the non-commutative interplay between the positive block σ_i^2 and the negative block σ_{i+1}^{-1} . At $t = -1$, the Burau matrices for inverse generators introduce negative entries; Perron–Frobenius no longer applies to the product, and the dominant eigenvalue need not be real. This sign interference means that *rearranging* the same generators changes the spectral radius in ways that the Abelian gate-count cannot track, exactly the blindness formalised in Theorem 6.2. For positive-only words (no σ_i^{-1}) the matrices are non-negative; Perron–Frobenius guarantees a real dominant eigenvalue and the Abelian rate is a tighter proxy. The discriminator gap that justifies the non-Abelian Burau pipeline is therefore widest precisely at the mixed-sign gate word $\sigma_i^2 \sigma_{i+1}^{-1}$.

4 Burau Representation and Lyapunov Exponent

The construction of Section 3 produces a braid word that grows longer with each epoch of the random walk. This word is an algebraic object (a sequence of generators and their inverses), not a number. To extract a quantitative risk signal, we need a way to measure how “tangled” the braid has become after T steps.

The Burau representation provides exactly this. It maps each braid generator to a matrix, converting the braid word into a matrix product. As the walk progresses and the braid word grows, we multiply one more matrix into the running product. The key question becomes: *does this product grow?* If the matrices merely rotate (eigenvalues on the unit circle), the product stays bounded and the braid is “flat”. But if the product grows exponentially, the braid is genuinely tangled: each new crossing compounds the complexity of all previous crossings. The rate of this exponential growth is the Lyapunov exponent, our primary risk metric.

The full Burau computation ($N \times N$ matrices, N simultaneous NHI walkers) is the authoritative discriminator of the focused/dispersed boundary and the calibration oracle against which the Abelian rate is evaluated. In operational deployment, temporal braid LE is the primary screening instrument; the Burau pipeline provides the ground truth for confirming the focused/dispersed classification in flagged ratchets where the Abelian rate may be biased.

4.1 Burau at $t = -1$: exact integer computation

Definition 4.1 (Unreduced Burau representation). The *unreduced Burau representation* $\rho_t : B_n \rightarrow \text{GL}_n(\mathbb{Z}[t, t^{-1}])$ maps each generator to:

$$\rho_t(\sigma_i) = I_n - t E_{ii} + t E_{i,i+1} + E_{i+1,i} - E_{i+1,i+1},$$

where E_{jk} is the matrix unit with 1 in position (j, k) and 0 elsewhere.

At the specialisation $t = -1$, each entry of $\rho_{-1}(\sigma_i)$ is an integer:

$$\rho_{-1}(\sigma_i)_{jk} = \begin{cases} 2 & j = k = i, \\ -1 & j = i, k = i + 1, \\ 1 & j = i + 1, k = i, \\ 0 & j = k = i + 1, \\ 1 & j = k \notin \{i, i + 1\}, \\ 0 & \text{otherwise.} \end{cases}$$

All subsequent matrix products remain integer-valued, enabling exact computation throughout the walk.

Working in exact integer arithmetic provides a significant numerical advantage over a float64 implementation. The spectral radius of the accumulated Burau product grows as $(2 + \sqrt{3})^M$

where M is the number of gate firings; at $T = 50$ epochs with a typical firing rate, M can reach several hundred, making $(2 + \sqrt{3})^M \sim 10^{200}$, which exceeds the float64 maximum ($\approx 1.8 \times 10^{308}$) for dense ratchets with high firing rates. Float64 representations would overflow to `inf`, yielding no usable spectral radius.

In Python, the language we use for our calculus, arbitrary-precision integers never overflow: matrix entries grow large but remain exact, and the characteristic polynomial is computed exactly over \mathbb{Z} . The only numerical step is the final eigenvalue extraction from an exact integer matrix, which is performed in floating point on a matrix whose entries are already determined exactly. This design is both the source of the 2.83% overflow rows reported in Section 7 (which arise from fixed-width integer limits in the dataset pipeline, not from the algorithm itself) and the reason the remaining 97.17% carry ground-truth spectral radii rather than float64 approximations.

4.2 Spectral radius and Lyapunov exponent

After a walk of length T producing permission braid $\beta = \sigma_{i_1}^{\epsilon_1} \cdots \sigma_{i_k}^{\epsilon_k}$, the *accumulated Burau matrix* is $\mathbf{B}(T) = \prod_{j=1}^k \rho_{-1}(\sigma_{i_j}^{\epsilon_j})$, and its *spectral radius* is $\text{SR}(T) = \max\{|\lambda| : \lambda \text{ eigenvalue of } \mathbf{B}(T)\}$.

Definition 4.2 (Lyapunov exponent). The *Lyapunov exponent* of SCC C under WAR assignment W is

$$\text{LE}(C, W) = \frac{\log \text{SR}(T_{\text{high}}) - \log \text{SR}(T_{\text{low}})}{T_{\text{high}} - T_{\text{low}}},$$

estimated over a walk of total length T_{high} with $T_{\text{low}} = T_{\text{high}}/2$.

Definition 4.3 (T -scaling ratio). The *T -scaling ratio* is

$$r = \frac{\Delta \log \text{SR}(T_{\text{high}})}{\Delta \log \text{SR}(T_{\text{low}})}, \quad \Delta \log \text{SR}(T) = \log \text{SR}(T) - \log \text{SR}(T/2).$$

Values of r near 1 indicate stable exponential scaling; values significantly below 1 indicate subexponential or transient growth.

Why exponential growth is stable. The NHI walkers form an irreducible finite Markov chain on the SCC, so the gate-firing process is ergodic. The sequence $a_T = \log \|\mathbf{B}(T)\|$ is subadditive by submultiplicativity of matrix norms, and the shift that advances the walk by one epoch preserves the stationary measure. Kingman’s subadditive ergodic theorem [10] therefore guarantees that $\frac{1}{T} \log \|\mathbf{B}(T)\|$ converges almost surely to a deterministic limit LE, independent of the walkers’ starting positions. Finite-state irreducibility ensures rapid mixing, explaining why LE stabilises within a few dozen gate firings in practice.

4.3 Firing-rate lower bound for hub-concentrated topologies

The preceding discussion established that LE grows with the gate-firing rate, but no formal lower bound linked graph topology to that rate. This subsection proves such a bound for a natural class of SCCs: those whose directed edges concentrate on a common high-privilege hub.

Definition 4.4 (k -hub SCC). Let $C = (V, E)$ be a ratchet SCC on $|V| = N$ vertices with WAR assignment W . A vertex $h \in V$ is a *k -hub* if there exist $k \geq 2$ distinct vertices $v_1, \dots, v_k \in V \setminus \{h\}$ such that:

1. Each $v_j \rightarrow h$ is a *directed* edge (i.e. $h \rightarrow v_j \notin E$), and
2. Each such edge is ascending: $W(h) > W(v_j)$ for all $j = 1, \dots, k$.

The *spoke set* is $S = \{v_1, \dots, v_k\}$ and each $v_j \rightarrow h$ is a *spoke edge*. Write d_j for the out-degree of v_j in the full graph C .

Definition 4.5 (Spoke-covered k -hub SCC). A k -hub SCC with spoke set $S = \{v_1, \dots, v_k\}$ is *spoke-covered* if every vertex $u \in V$ has at least one directed out-edge to the spoke set: for all $u \in V$, $\{j : u \rightarrow v_j \in E\} \neq \emptyset$.

Spoke coverage is the condition that the spoke set S is a *dominating set* of the directed graph: every vertex has at least one immediate out-neighbour in S . In permission-graph terms, it says that from any privilege state, some direct de-escalation path exists, a mild structural condition satisfied by any ratchet SCC in which the spoke vertices act as “gateway” low-privilege roles.

The random walk model (Section 3) places n walkers performing independent, uniform random walks on C . At each epoch, every walker at vertex u moves to a neighbour chosen uniformly at random from the d_u out-neighbours of u .

Lemma 4.6 (Spoke-step probability). *Let C be an SCC containing a k -hub h with spoke set $S = \{v_1, \dots, v_k\}$, and let d_{\max} denote the maximum out-degree in C . For n independent walkers, each performing a uniform random walk on C , let $X_{i,t}$ be the indicator that walker i takes a spoke step at epoch t , and define the ensemble spoke-step frequency*

$$\hat{p}_h = \frac{1}{nT} \sum_{i=1}^n \sum_{t=1}^T X_{i,t}.$$

Then the expected spoke-step probability satisfies:

(i) **Universal bound.**

$$p_h = \mathbb{E}[\hat{p}_h] \geq \frac{k}{|V| \cdot d_{\max}^{\text{diam}(C)+1}},$$

where $\text{diam}(C)$ is the diameter of the SCC.

(ii) **Spoke-covered bound.** *If C is spoke-covered (Theorem 4.5) and every vertex has out-edges to all k spoke vertices, then*

$$p_h \geq \frac{k}{d_{\max}^2},$$

independent of $|V|$ and $\text{diam}(C)$. Under the weaker spoke-coverage condition (each vertex has at least one out-edge to S), the bound is $p_h \geq 1/d_{\max}^2$.

The ensemble frequency concentrates around its mean:

$$\Pr[\hat{p}_h \leq p_h - \epsilon] \leq e^{-2n\epsilon^2} \quad \text{for all } \epsilon > 0.$$

Proof. See Section A. □

Lemma 4.7 (Spoke-pair event count). *Under the hypotheses of Theorem 4.6, let $m_{\text{spoke}}(t)$ denote the number of unordered pairs $\{i, j\}$ such that both walker i and walker j take a spoke step at epoch t . Then*

$$\mathbb{E}[m_{\text{spoke}}(t)] \geq \binom{n}{2} p_h^2 \geq \frac{n(n-1)}{2} \cdot \frac{k^2}{N^2 \cdot d_{\max}^{2(\text{diam}(C)+1)}}.$$

Proof. See Section A. □

Theorem 4.8 (Firing-rate lower bound for k -hub SCCs). *Let C be a ratchet SCC on $N = |V|$ vertices with a k -hub h (Theorem 4.4), and let n walkers perform independent uniform random walks on C in stationarity. Let p_h be the per-walker spoke-step probability from Theorem 4.6. Over a walk of T epochs, the expected number of gate-eligible firings satisfies*

$$\mathbb{E}[M_T] \geq T \cdot \left\lfloor \frac{n-1}{2} \right\rfloor \cdot p_h^2.$$

Substituting the two bounds from Theorem 4.6:

$$(i) \text{ **Universal:}** \mathbb{E}[M_T] \geq T \cdot \left\lfloor \frac{n-1}{2} \right\rfloor \cdot \frac{k^2}{N^2 \cdot d_{\max}^{2(\text{diam}(C)+1)}}.$$

$$(ii) \text{ **Spoke-covered:}** \mathbb{E}[M_T] \geq T \cdot \left\lfloor \frac{n-1}{2} \right\rfloor \cdot \frac{k^2}{d_{\max}^4}.$$

For the pipeline's $n = 6$ walkers, $\lfloor (n-1)/2 \rfloor = 2$, so $\mathbb{E}[M_T] \geq 2T \cdot p_h^2$ in both cases.

Proof. See Section A. □

Corollary 4.9 (Counting-LE lower bound for k -hub SCCs). *Under the hypotheses of Theorem 4.8, the counting Lyapunov exponent (the LE that would result if each gate firing contributed exactly $\log(2 + \sqrt{3})$ to $\log \text{SR}$) satisfies*

$$\text{LE}_{\text{count}} \geq \frac{\mathbb{E}[M_T]}{T} \cdot \log(2 + \sqrt{3}) \geq 2p_h^2 \cdot \log(2 + \sqrt{3}).$$

Substituting the two bounds from Theorem 4.6 (with $n = N = 6$):

(i) **Universal** (SCC diameter $D = \text{diam}(C)$):

$$\text{LE}_{\text{count}} \geq \frac{k^2 \cdot \log(2 + \sqrt{3})}{2 \cdot N^2 \cdot d_{\max}^{2(D+1)}}.$$

(ii) **Spoke-covered** (every vertex has out-edges to all k spokes, independent of N and D):

$$\text{LE}_{\text{count}} \geq \frac{k^2 \cdot \log(2 + \sqrt{3})}{2 \cdot d_{\max}^4}.$$

Proof. See Section A. □

Tightness and the temporal correction. Both bounds in Theorem 4.9 are on the *counting* LE, which is an overestimate of the true (temporal) LE: the shuffling experiment (Section 5.2) shows temporal ordering produces systematic spectral cancellation, with temporal SR below shuffled SR in 84% of pairs. The bounds therefore provide conservative floors on $\text{LE}_{\text{temporal}}$ and should be read as order-of-magnitude indicators rather than tight guarantees. The median relative gap between counting and temporal LE is only 1.3% (Section 5.2), so the bounds remain useful for identifying clearly high-risk topologies.

5 Braid Non-Commutativity and the Shuffling Experiment

A natural question is whether the temporal ordering of gate-firing injections matters for LE, or whether LE reduces to a simple function of the gate-firing count. This section shows that the ordering carries genuine non-commutative signal.

5.1 Algebraic structure of injection-triplet products

Let T_i denote the Burau matrix of a single injection triplet $\sigma_i^2\sigma_{i+1}^{-1}$ at position i . Direct computation at $t = -1$ gives:

- **Same position:** $\text{SR}(T_i \cdot T_i) = (2 + \sqrt{3})^2 \approx 13.93$. Growth is fully multiplicative.
- **Adjacent positions ($|i - j| = 1$):** $\text{SR}(T_i \cdot T_j) = 1$. The product has all eigenvalues on the unit circle (complete spectral cancellation).
- **Gap-2 positions ($|i - j| = 2$):** $\text{SR}(T_i \cdot T_j) \approx 7.09$. Growth is partially retained but the matrices do not commute: $\|T_i T_j - T_j T_i\|_F \approx 7.48$.

The adjacent-pair guard (Section 3.4) prevents adjacent-position firings within a single epoch, so within-epoch products are always at non-adjacent (gap ≥ 2) triplet positions. Because the guard scans positions left-to-right and skips position $i + 1$ whenever position i fires, the within-epoch firing order is fixed by the scan; there is no ordering degree of freedom to exploit. Non-commutativity arises *across* epochs, when different positions fire in consecutive epochs.

Strand count matters. With n strands there are $n - 2$ generator $\sigma_i^2\sigma_{i+1}^{-1}$ positions. At $n = 4$ (2 positions, always adjacent), every cross-position product gives $\text{SR} = 1$; the guard forces single-position dominance and the permission braid collapses to a power of one matrix: ordering becomes trivially irrelevant. At $n = 6$ (4 positions), gap-2 pairs (0, 2) and (1, 3) produce non-commuting products ($\text{SR} \approx 7.09$, $\|[T_i, T_j]\|_F \approx 7.48$), while the gap-3 pair (0, 3) commutes but still has $\text{SR} > 1$. Together these restore genuine cross-epoch ordering dependence. Our pipeline uses $n = 6$ strands (matching one NHI per SCC vertex).

5.2 Shuffling experiment

We ran 469 (SCC, WAR) pairs across all 82 ratchet topologies with 6 NHIs (4 generator positions). For each pair, 30 random walks of 100 epochs were performed. Each walk's braid word was decomposed into injection triplets, then:

1. **Original:** log SR of the temporal-order braid.
2. **Shuffled:** triplets uniformly permuted at random (20 shuffles per walk, averaged).
3. **Position-sorted:** triplets grouped by generator position (all position-0 firings first, then position-1, etc.), eliminating cross-position temporal cancellation.

Statistic	Value
(SCC, WAR) pairs	469
<i>Original vs. Shuffled</i>	
Paired t -statistic	-15.0
Cohen’s d	-0.69
Fraction (orig < shuffled)	84 %
Median relative difference	1.3 %
<i>Original vs. Position-Sorted</i>	
Fraction (orig < sorted)	97 %
Mean (orig - sorted) / orig	-21.5 %
<i>Position diversity</i>	
Walks with ≥ 2 distinct positions	95.3 %

The temporal ordering produces a **significant, systematic** reduction in SR compared to both shuffled and sorted baselines ($t = -15.0$, $d = -0.69$, $p \ll 10^{-30}$). Temporal braids have lower SR in 84% of pairs, and 22% lower than position-sorted braids on average.

5.3 Interpretation: spectral cancellation as signal

The direction of the effect (temporal ordering *reduces* SR) has a clean explanation. In the temporal braid, a walker that fires at position i in epoch t is likely to fire at a nearby position in epoch $t + 1$ (since strands move locally). These cross-epoch adjacent-position interactions produce partial spectral cancellation ($\text{SR}(T_i \cdot T_{i\pm 1}) = 1$). Shuffling randomises these interactions, breaking the temporal correlation and eliminating the systematic cancellation.

This effect is not noise: it carries structural information about the SCC. Topologies where directed edges cluster in adjacent regions of the braid produce more cross-epoch cancellation and therefore lower LE at the same firing rate. The temporal braid captures this spatial structure; the shuffled braid destroys it.

5.4 Temporal LE is a better discriminator than gate-firing count

A natural objection is that if the firing rate explains most of the variance in LE, the full Bureau validation machinery is overkill: one could simply count gate firings and multiply by $\log(2 + \sqrt{3})$. We refute this with three tests.

Test 1: Partial correlation with DWS. DWS is computed from topology and WAR alone, independent of the Bureau validation computation. We compute $r(\text{LE}, \text{DWS} \mid n_{\text{trips}})$, the Pearson correlation between LE and DWS after linearly removing the effect of the gate-firing count.

LE variant	$r(\text{LE}, \text{DWS} \mid n_{\text{trips}})$	p
LE _{temporal}	0.175	1.5×10^{-4}
LE _{counting}	0.001	0.98
LE _{shuffled}	0.149	1.2×10^{-3}

After removing firing-rate variance, **counting LE retains zero correlation with DWS** ($r = 0.001$, $p = 0.98$). Temporal LE retains $r = 0.175$ ($p < 10^{-3}$). The non-commutative correction carries structural information that counting cannot capture.

Test 2: Matched-rate spread. Grouping pairs into firing-rate bins (± 5 triplets) and measuring the within-bin LE range shows that temporal LE consistently exhibits **3–4× more spread** than counting LE at the same firing rate. For example, at ≈ 90 triplets per walk ($n = 40$ pairs): temporal range = 0.534, counting range = 0.127. This additional spread reflects structural differences between SCCs that share a firing rate but differ in the spatial distribution of their directed edges.

Test 3: DWS-sign Fisher ratio. Using DWS sign (positive vs. non-positive) as an external discriminant axis independent of the Bureau computation:

LE variant	Fisher ratio (DWS>0 vs. DWS≤0)
LE _{temporal}	0.088
LE _{shuffled}	0.083
LE _{counting}	0.061

Temporal LE separates DWS-sign groups 45% better than counting LE.

6 Two-Regime Classification

6.1 LE as the sole regime discriminator

Each ratchet deployment, a specific (C, W) pair, is assigned to one of two dynamical regimes by a single quantity: the Lyapunov exponent LE of the accumulated Bureau matrix product.

LE (**primary signal**) captures *structural risk*: how fast does the permission braid spectral radius grow per step? It is determined by the graph topology (density of directed edges, hub connectivity) and by the WAR assignment (which edges are traversed in ascending order). Its value encodes whether non-commutative cancellations between consecutive gate firings dominate (low LE, focused regime) or whether crossings accumulate without cancellation (high LE, dispersed regime).

Definition 6.1 (Two-regime classification). Each ratchet deployment (C, W) belongs to exactly one of two regimes, separated at the corpus median LE = 0.5847 (the median of per-SCC mean LE across the 1000-SCC corpus, chosen so that the two regimes are equally represented under a random-SCC assumption):

	LE
LE < 0.5847	focused
LE ≥ 0.5847	dispersed

The reason why we are choosing the median is that given a random uniform sample of SCCs, there is no bias towards either topology.

Regime	Topology	Remediation
focused	Escalation channelled, few paths	WAR reassignment
dispersed	Hub-rich, multiple independent paths	Topology restructuring

Table 1: Two-regime classification with remediation paths.

The **dispersed** regime ranks highest because it persists across WAR assignments: hub topologies sustain the gate regardless of privilege alignment, so no WAR reassignment suppresses escalation. Only adding or reversing directed edges (topology surgery) suffices.

The **focused** regime is WAR-controlled: the current assignment aligns directed edges with ascending privilege flow, driving spectral growth. Reassigning WAR to break that alignment reduces LE and remediates the ratchet without touching the graph structure.

The Directed WAR Sum $DWS(C, W) = \sum_{(u \rightarrow v) \in E_{\text{dir}}} (W(v) - W(u))$ is a static, $O(|E_{\text{dir}}|)$ abelian statistic that measures net uphill privilege flow under the current assignment. $DWS > 0$ indicates that directed edges run net-uphill, amplifying gate activity; $DWS \leq 0$ indicates suppression. Within the focused regime, DWS helps identify the specific WAR reassignment that remediates the deployment. However, DWS is an abelian count and cannot determine LE: two deployments with the same DWS and the same gate-firing rate can have different LE values and therefore belong to different regimes. LE must be determined by a non-abelian instrument (Section 6.1).

Proposition 6.2 (Abelian blindness). *No function of the abelian statistics of a ratchet walk (generator frequencies, gate-firing rate, or DWS) determines the Lyapunov exponent LE.*

Proof. The Lyapunov exponent $LE = \lim_{T \rightarrow \infty} \frac{1}{T} \mathbb{E}[\log \|\rho(g_T) \cdots \rho(g_1)\|]$ is a property of the *joint* distribution of the random matrix sequence, not of its one-dimensional marginals (the generator frequencies). Any abelian statistic is a function of those marginals alone. Since the Burau matrices for adjacent generators do not commute, rearranging the *order* of generators, while preserving their multiset, changes the spectral growth rate.

Explicit witness. In B_3 at the specialisation $t = -1$, set $A = \rho(\sigma_1) = \begin{pmatrix} 1 & 1 \\ 0 & 1 \end{pmatrix}$ and $C = \rho(\sigma_2^{-1}) = \begin{pmatrix} 1 & 0 \\ 1 & 1 \end{pmatrix}$. Both are integer upper/lower-triangular matrices; their product is not the identity ($AC \neq CA$). Consider the two words of length 5:

$$\begin{aligned} w_1 &= \sigma_1^3 \sigma_2^{-2}, & \rho(w_1) &= A^3 C^2 = \begin{pmatrix} 7 & 3 \\ 2 & 1 \end{pmatrix}, & \text{SR}(\rho(w_1)) &= 4 + \sqrt{15}; \\ w_2 &= (\sigma_1 \sigma_2^{-1})^2 \sigma_1, & \rho(w_2) &= (AC)^2 A = \begin{pmatrix} 5 & 8 \\ 3 & 5 \end{pmatrix}, & \text{SR}(\rho(w_2)) &= 5 + 2\sqrt{6}. \end{aligned}$$

Both words have identical abelian image $(3, -2) \in \mathbb{Z}^2$ (three σ_1 's and two σ_2^{-1} 's), so every abelian statistic (gate-firing rate, DWS, exponent sums) agrees. Yet $4 + \sqrt{15} \approx 7.87 \neq 9.90 \approx 5 + 2\sqrt{6}$, so the periodic walks repeating w_1 and w_2 have Lyapunov exponents $\frac{1}{5} \log(4 + \sqrt{15}) \approx 0.413$ and $\frac{1}{5} \log(5 + 2\sqrt{6}) \approx 0.459$ per step, respectively. No abelian statistic can distinguish them. \square

Corollary 6.3 (Telescoping blindness for directed cycles). *Let $v_1 \rightarrow v_2 \rightarrow \cdots \rightarrow v_k \rightarrow v_1$ be a directed cycle embedded in a ratchet SCC (C, W) . The contribution of this cycle to DWS is identically zero for every WAR assignment W :*

$$DWS_{\text{cycle}}(W) = \sum_{i=1}^k (W(v_{i+1 \bmod k}) - W(v_i)) = 0.$$

No WAR assignment can make a directed cycle net-ascending ($DWS_{\text{cycle}} > 0$) or net-descending ($DWS_{\text{cycle}} < 0$): the cycle is DWS-neutral by construction.

Although the cycle's net privilege flow is always zero, individual edges within it can be ascending or descending depending on the WAR assignment. Whenever at least one cycle edge is ascending, the gate fires on that edge, injecting non-commuting braid generators that drive spectral growth. A directed cycle with r ascending edges fires r gate events per traversal while contributing exactly zero to DWS, so the abelian pre-filter is permanently blind to the cycle's escalation potential regardless of WAR.

Proof. The sum telescopes: $(W(v_2) - W(v_1)) + (W(v_3) - W(v_2)) + \cdots + (W(v_1) - W(v_k)) = W(v_1) - W(v_1) = 0$. Since the WAR values appear and cancel in adjacent pairs around the cycle, the result holds for every choice of W . \square

Abelian statistics (DWS, gate-firing rate) are blind to the *order* in which directed edges are traversed and therefore cannot detect the non-commutative cancellations that define the focused/dispersed boundary. Two deployments with identical DWS and firing rate can have different LE values: one focused (cancellations dominate), one dispersed (crossings accumulate), with opposite remediations.

Theorem 6.3 gives the sharpest structural instance of this blindness. A directed cycle contributes exactly zero to DWS for *every* WAR assignment simultaneously; it is not that a specific unlucky assignment happens to cancel: the cancellation is topological and unavoidable. Any SCC whose directed edges include a cycle will therefore have a DWS-invisible escalation channel that the permission braid can detect but the abelian pre-filter never will.

Regime as a deployment property. The two regimes classify a *deployment*, not a topology alone. Two SCCs with identical primordial invariant R (same fusion class) may sit in different regimes if their WAR assignments differ. Conversely, the same SCC observed at different epochs may transition between regimes as its WAR assignment drifts. This is precisely the operational value of the braid framework: topology screening (primordial) identifies ratchets, but deployment screening (Bureau LE) identifies which ratchets are actively dangerous and which kind of intervention is required.

7 Empirical Validation

7.1 Dataset

The validation dataset [9] covers 1,000 ratchet SCC topologies generated at random from the set of all 6-vertex SCC topologies, each a directed-mixed graph combining directed and bidirectional edges. For each topology, 50 WAR assignments $(W_0, \dots, W_5) \in \{0, \dots, 5\}^6$ are sampled uniformly at random and evaluated with the braid walk simulator at $T = 50$ epochs and $w = 64$ walks, yielding **49,972** (SCC, WAR) pairs in total.

Two independent regime labels are computed per pair:

- **Bureau LE:** dispersed if $LE > 0.5847$, focused otherwise. The threshold is the median of the per-SCC mean LE across the full 1,000-SCC corpus.
- **Abelian rate:** dispersed if $le_counting > 0.6586$, focused otherwise, with the threshold set identically as the corpus median of per-SCC mean rates.

Across all 49,972 pairs, **2,852 (5.7%)** exhibit a regime disagreement between the two metrics. The two error directions are nearly symmetric: 1,418 *FD* cases (Focused by Bureau, Dispersed by rate; Bureau says the deployment is manageable, rate raises a false alarm) and 1,434 *DF* cases (Dispersed by Bureau, Focused by rate; Bureau detects genuine non-commutative growth that the abelian rate misses). This near-symmetry at the corpus level conceals a sharply topology-dependent pattern: individual SCCs are strongly skewed toward one error type, and the skew direction is governed by whether the topology’s directed edges concentrate crossings on a single braid strand position or fan out to produce diverse non-commuting generators.

At $T = 50$ epochs, 1,412 rows (2.83%) encounter integer arithmetic overflow in the Bureau matrix product; these rows record $LE = le_counting = 0$ and therefore agree trivially on the focused label, contributing zero disagreements. No SCC has all 50 WAR samples overflowed, and all four case-study SCCs below are overflow-free.

7.2 Case studies

The four subsections that follow use ratchet topologies drawn directly from the synthetic corpus. They are ordered by failure mode: **SCC 216** (9 dir, 2 bidir) shows pure FD failures: directed

edges concentrate ascending crossings on a small set of strand positions, and the abelian rate consistently over-calls dispersed. **SCC 207** (10 dir, 4 bidir) shows pure DF failures: a bidir hub at v_1 distributes crossing events across diverse strand positions, driving Burau growth that the abelian rate misses. **SCC 126** (9 dir, 3 bidir) sits at the transition: depending on WAR assignment, the topology produces either FD or DF failures with equal frequency. **SCC 233** (6 dir, 5 bidir) shows pure DF failures despite having more bidirectional than directed edges, driven by a directed 4-cycle whose WAR contributions telescope to zero while its braid generators grow exponentially.

7.3 SCC 216: Directed Fan-Out Hub, FD-Only

SCC 216 has 9 directed and 2 bidirectional edges. The directed edges are $v_1 \rightarrow v_0$, $v_0 \rightarrow v_2$, $v_0 \rightarrow v_3$, $v_1 \rightarrow v_2$, $v_3 \rightarrow v_1$, $v_5 \rightarrow v_1$, $v_3 \rightarrow v_4$, $v_3 \rightarrow v_5$, $v_4 \rightarrow v_5$; the bidirectional edges are $v_2 \leftrightarrow v_4$ and $v_2 \leftrightarrow v_5$. The dominant structural feature is v_3 as a directed fan-out hub: it sends edges to v_1 , v_4 , and v_5 , while itself receiving only from $v_0 \rightarrow v_3$. Ascending crossings from v_3 repeatedly land on v_3 's strand, and the two bidir edges ($v_2 \leftrightarrow v_4$, $v_2 \leftrightarrow v_5$) oscillate locally without diversifying generator strand positions.

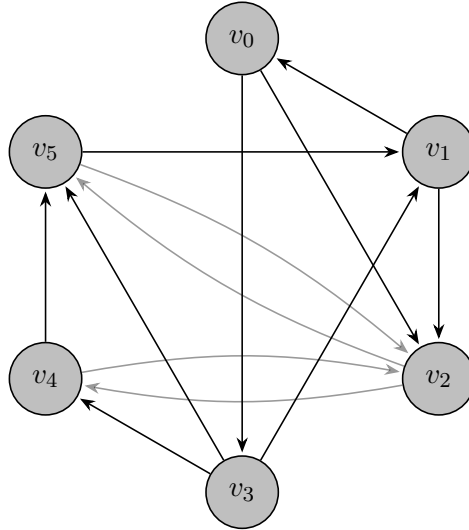


Figure 3: SCC 216: 9 directed (solid) and 2 bidirectional edges (paired, 40% opacity). v_3 is the directed fan-out hub; $v_2 \leftrightarrow v_4$ and $v_2 \leftrightarrow v_5$ are local bidir oscillators.

Out of 50 WAR samples, **6 are FD** and **0 are DF** (thresholds $\theta_{LE} = 0.5847$, $\theta_{rate} = 0.6586$). The abelian rate consistently over-calls dispersed; Burau never over-calls.

WAR (W_0, \dots, W_5)	LE	rate	type
(0, 2, 0, 0, 3, 4)	0.460	0.675	FD
(0, 3, 0, 0, 4, 5)	0.471	0.689	FD
(4, 2, 1, 2, 4, 2)	0.532	0.858	FD
(5, 0, 0, 5, 4, 0)	0.551	0.793	FD
(4, 0, 0, 3, 5, 0)	0.570	0.910	FD
(1, 1, 0, 5, 2, 5)	0.509	0.921	FD

Table 2: FD disagreements for SCC 216 (no DF failures). FD: LE < 0.5847 (focused by Burau) and rate > 0.6586 (dispersed by abelian counter).

Why only FD? In every FD case WAR elevates v_3 or its targets (v_4, v_5) to high WAR, causing ascending crossings from $v_3 \rightarrow v_1, v_3 \rightarrow v_4, v_3 \rightarrow v_5$ to fire the gate repeatedly. The abelian counter tallies each gate-fire and reports high rate. The Burau product, however, accumulates generators at a concentrated set of strand positions: v_3 is the structural origin of nearly every directed crossing, so all injected braid generators commute or nearly commute. Repeated applications of generators at the same strand position are not exponentially amplifying; spectral radius stays subcritical ($LE < 0.5847$ across all 6 FD cases, reaching 0.570 at most). DF failure never occurs because the bidir connections of v_2 ($v_2 \leftrightarrow v_4, v_2 \leftrightarrow v_5$) do not create diverse independent crossing chains: no WAR assignment can route flow through enough distinct strand positions to drive exponential non-commutative growth.

7.4 SCC 207: Bidir Hub Diversifies Generators, DF-Only

SCC 207 has 10 directed and 4 bidirectional edges. The directed edges are $v_0 \rightarrow v_2, v_3 \rightarrow v_0, v_4 \rightarrow v_0, v_0 \rightarrow v_5, v_3 \rightarrow v_1, v_2 \rightarrow v_3, v_4 \rightarrow v_2, v_2 \rightarrow v_5, v_3 \rightarrow v_5, v_4 \rightarrow v_5$; the bidirectional edges are $v_0 \leftrightarrow v_1, v_1 \leftrightarrow v_2, v_1 \leftrightarrow v_5, v_3 \leftrightarrow v_4$. Node v_1 is the bidir hub, connected bidirectionally to $v_0, v_2,$ and v_5 ; nodes v_3 and v_4 share a bidir link while each sending multiple directed edges outward.

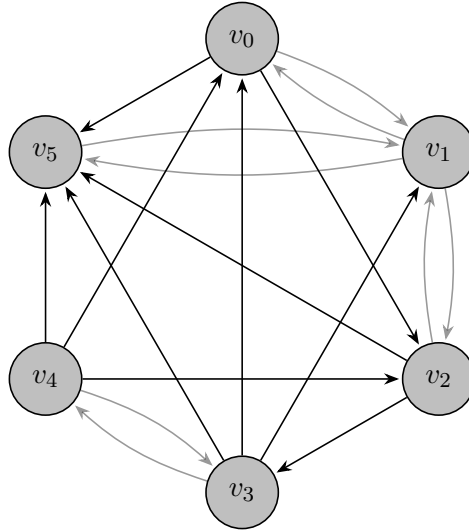


Figure 4: SCC 207: 10 directed (solid) and 4 bidirectional edges (paired, 40% opacity). v_1 is the bidir hub connected to v_0, v_2, v_5 ; v_3 and v_4 are directed fan-out sources sharing a bidir link.

Out of 50 WAR samples, **0 are FD** and **5 are DF**. The abelian rate never over-calls dispersed; Burau consistently detects non-commutative growth that the rate misses.

WAR (W_0, \dots, W_5)	LE	rate	type
(1, 3, 5, 0, 5, 2)	0.585	0.618	DF
(4, 5, 1, 4, 5, 3)	0.596	0.635	DF
(0, 0, 5, 5, 2, 4)	0.618	0.638	DF
(0, 0, 5, 3, 2, 2)	0.591	0.611	DF
(0, 3, 3, 2, 5, 2)	0.630	0.653	DF

Table 3: DF disagreements for SCC 207 (no FD failures). DF: $LE > 0.5847$ (dispersed by Burau) and $rate < 0.6586$ (focused by abelian counter).

Why only DF? In each DF case WAR distributes so that v_3 or v_4 (directed fan-out sources) are elevated relative to v_0, v_2, v_5 . The directed edges $v_3 \rightarrow v_0, v_4 \rightarrow v_0, v_3 \rightarrow v_1, v_4 \rightarrow v_2, v_3 \rightarrow v_5,$

$v_4 \rightarrow v_5$ fan out to five different target nodes, each occupying a distinct strand position in the braid. The bidir hub v_1 adds further crossing diversity by oscillating between v_0 , v_2 , and v_5 at different WAR levels. The combined effect is a braid word with generators at many independent positions; non-commuting products accumulate and Burau detects spectral growth ($LE > 0.5847$). The abelian counter, however, sees near-balanced directed flow in these cases (rates marginally below threshold), classifying as focused while the non-commutative structure grows exponentially. FD failure never occurs because the fan-out structure always distributes crossing events across enough strand positions to prevent generator repetition from dominating the Burau product.

7.5 SCC 126: Dual-Source Hub, Balanced FD and DF

SCC 126 has 9 directed and 3 bidirectional edges. The directed edges are $v_1 \rightarrow v_0$, $v_0 \rightarrow v_3$, $v_5 \rightarrow v_0$, $v_1 \rightarrow v_2$, $v_1 \rightarrow v_4$, $v_5 \rightarrow v_1$, $v_3 \rightarrow v_2$, $v_5 \rightarrow v_2$, $v_3 \rightarrow v_5$; the bidirectional edges are $v_2 \leftrightarrow v_4$, $v_3 \leftrightarrow v_4$, $v_4 \leftrightarrow v_5$. The topology has two major directed sources: v_1 (sending to v_0 , v_2 , v_4) and v_5 (sending to v_0 , v_1 , v_2). Node v_4 is the bidir hub, connected bidirectionally to v_2 , v_3 , and v_5 .

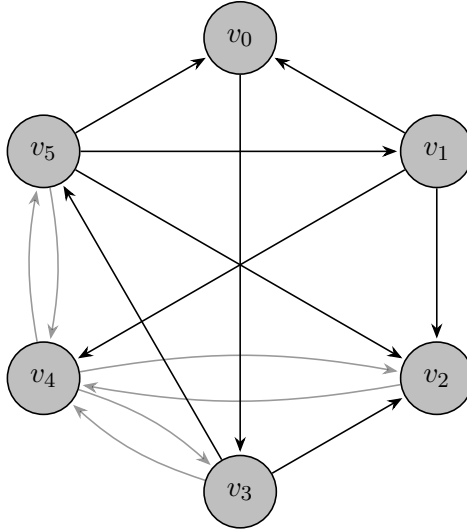


Figure 5: SCC 126: 9 directed (solid) and 3 bidirectional edges (paired, 40% opacity). v_1 and v_5 are dual directed sources; v_4 is the bidir hub.

Out of 50 WAR samples, **3 are FD** and **3 are DF**, the most balanced split of the four case studies.

WAR (W_0, \dots, W_5)	LE	rate	type
(5, 1, 0, 2, 0, 2)	0.468	0.681	FD
(4, 3, 2, 5, 2, 3)	0.428	0.746	FD
(3, 2, 4, 3, 3, 3)	0.546	0.785	FD
(1, 1, 3, 5, 5, 5)	0.605	0.648	DF
(2, 3, 3, 4, 0, 3)	0.638	0.651	DF
(0, 2, 1, 5, 2, 5)	0.604	0.614	DF

Table 4: Disagreements for SCC 126. FD: $LE < 0.5847$ and $rate > 0.6586$; DF: $LE > 0.5847$ and $rate < 0.6586$.

FD failures: v_1 as a crossing funnel. In the FD cases (e.g. $(4, 3, 2, 5, 2, 3)$, $LE=0.428$, $rate = 0.746$) WAR elevates v_3 to the highest rank while v_1 has intermediate WAR. Directed edges $v_5 \rightarrow v_1$, $v_3 \rightarrow v_2$, and $v_3 \rightarrow v_5$ produce ascending crossings that land repeatedly near v_3 's strand position. The abelian counter accumulates many ascending events and reports high rate. The Burau product, however, sees generators concentrated at the strand corresponding to v_3 ; repeated identical generators do not drive spectral growth ($LE=0.428$).

DF failures: v_5 and v_4 activate diverse chains. In the DF cases (e.g. $(1, 1, 3, 5, 5, 5)$, $LE=0.605$, $rate = 0.648$) WAR elevates both v_3 , v_4 , and v_5 to high WAR. Now $v_5 \rightarrow v_0$, $v_5 \rightarrow v_1$, $v_5 \rightarrow v_2$, and the bidir $v_4 \leftrightarrow v_5$ crossings span five distinct strand positions. The diverse generators produce non-commuting products; Burau detects spectral growth ($LE=0.605$) while the abelian rate, seeing near-balanced directed flow, falls just below the dispersed threshold.

Hub as regime switch. The balanced FD/DF split arises from the interplay of v_1 and v_5 : when WAR concentrates flow through v_1 , it becomes a crossing funnel \Rightarrow FD; when WAR distributes to activate v_5 's fan-out plus v_4 's bidir connections, generator diversity drives exponential Burau growth \Rightarrow DF. The abelian rate is blind to this distinction in both directions.

7.6 SCC 233: Directed 4-Cycle Within Bidir-Heavy Topology, DF-Only

SCC 233 has 6 directed and 5 bidirectional edges. Despite having more bidirectional than directed edges (an unusual configuration), it exhibits **0 FD** and **7 DF** failures out of 50 WAR samples.

The directed edges are $v_0 \rightarrow v_1$, $v_4 \rightarrow v_0$, $v_5 \rightarrow v_0$, $v_3 \rightarrow v_1$, $v_1 \rightarrow v_5$, $v_5 \rightarrow v_4$; the bidirectional edges are $v_0 \leftrightarrow v_3$, $v_1 \leftrightarrow v_2$, $v_1 \leftrightarrow v_4$, $v_2 \leftrightarrow v_4$, $v_3 \leftrightarrow v_5$. The defining structural feature is the directed 4-cycle $v_0 \rightarrow v_1 \rightarrow v_5 \rightarrow v_4 \rightarrow v_0$, embedded within a bidir-rich neighbourhood.

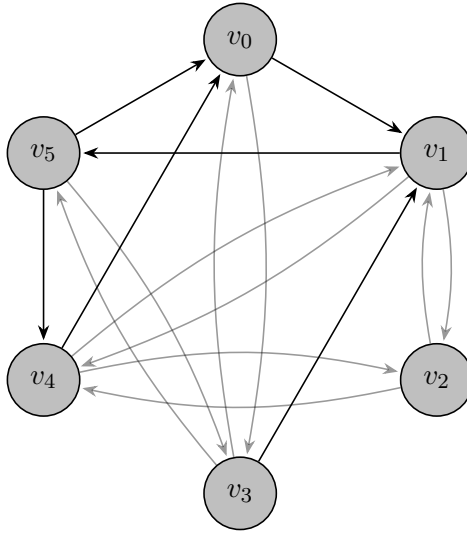


Figure 6: SCC 233: 6 directed (solid) and 5 bidirectional edges (paired, 40% opacity). Directed 4-cycle $v_0 \rightarrow v_1 \rightarrow v_5 \rightarrow v_4 \rightarrow v_0$ is the source of DF failures; bidir edges $v_1 \leftrightarrow v_2$, $v_1 \leftrightarrow v_4$, $v_2 \leftrightarrow v_4$ form a local triangle.

Why only DF? Theorem 6.3 provides the structural explanation. The four directed cycle edges $v_0 \rightarrow v_1 \rightarrow v_5 \rightarrow v_4 \rightarrow v_0$ form a closed loop, so their WAR differences telescope to exactly zero:

$$DWS_{\text{cycle}} = (W(v_1) - W(v_0)) + (W(v_5) - W(v_1)) + (W(v_4) - W(v_5)) + (W(v_0) - W(v_4)) = 0$$

WAR (W_0, \dots, W_5)	LE	rate	type
(1, 4, 5, 2, 3, 3)	0.587	0.600	DF
(2, 3, 1, 3, 5, 1)	0.601	0.625	DF
(0, 4, 2, 1, 4, 2)	0.606	0.635	DF
(4, 4, 4, 4, 3, 1)	0.627	0.657	DF
(2, 3, 5, 5, 2, 1)	0.603	0.656	DF

Table 5: DF disagreements for SCC 233 (no FD failures; 2 of 7 rows omitted for brevity). DF: LE > 0.5847 (dispersed by Bureau) and rate < 0.6586 (focused by abelian counter).

for *every* WAR assignment. This is a topological identity that holds unconditionally, not a coincidental numerical cancellation. The abelian rate therefore sees the cycle’s contribution as permanently neutral; it can only report dispersed based on the two non-cycle directed edges ($v_5 \rightarrow v_0$ and $v_3 \rightarrow v_1$), which in the DF cases nearly cancel or fall below threshold.

Yet the cycle still fires the gate on its ascending edges. In (1, 4, 5, 2, 3, 3): $v_0=1$, $v_1=4$, so $v_0 \rightarrow v_1$ is ascending; $v_1=4$, $v_5=3$, so $v_1 \rightarrow v_5$ is descending; $v_5=3$, $v_4=3$, so $v_5 \rightarrow v_4$ is flat; $v_4=3$, $v_0=1$, so $v_4 \rightarrow v_0$ is descending. The ascending edge $v_0 \rightarrow v_1$ fires the gate, injecting braid generators. As walkers traverse the cycle, the four structurally distinct generator positions produce non-commuting products that accumulate exponentially (LE = 0.587). The bidir triangle $v_1 \leftrightarrow v_2 \leftrightarrow v_4 \leftrightarrow v_1$ adds further generator diversity at v_1 ’s strand without inflating the abelian rate.

FD failure never occurs because the telescoping identity prevents the cycle from contributing to the abelian rate: any WAR assignment that fires the cycle must produce a rate contribution near zero from cycle activity alone, so the abelian counter cannot over-call dispersed based on cycle crossings. The bidir-heavy neighbourhood could in principle produce FD by inflating the abelian rate, but bidir edges’ paired forward–reverse crossings cancel in DWS as well, providing no net directed-flow signal to over-count.

8 Discussion

8.1 Topology classification vs. deployment classification

The primordial invariant classifies *topologies*: it discriminates oscillators (no ratchet structure, topologically safe) from ratchets (directed WAR paths capable of monotone escalation). Two SCCs in the same primordial fusion class share identical cycle escalation profiles and receive one analyst review, the right level of abstraction for triage and whitelist management at scale.

The braid framework classifies *deployments*. It is applied *after* primordial screening, for SCCs already identified as ratchets. Its input is the topology together with the ground-truth WAR assignment; its output is LE, the non-abelian risk metric that abelian statistics cannot determine. LE alone partitions every ratchet deployment into focused or dispersed, the two regimes with distinct remediations. The two layers operate sequentially (see Section 9 for the full pipeline). This separation avoids redundant dynamic analysis: oscillators are filtered before any dynamic analysis runs.

8.2 Alternative Abelian baselines

The Abelian baseline used throughout this paper, gate-firing count and $|\text{DWS}|$, is intentionally simple: it represents the strongest signal available from a single linear scan of the directed edges under a given WAR assignment. A natural question is whether more sophisticated Abelian statistics could close the gap with temporal braid LE. We examine three candidates and show that none can substitute for the non-Abelian screen, for reasons that are structural (Theorem 6.2), empirical, or both.

Spectral gap of the transition matrix. The spectral gap $\gamma = 1 - \lambda_2(P)$ of the random-walk transition matrix P measures mixing speed: a large gap means fast mixing, so walkers move broadly across the SCC and diversify generator positions; a small gap means slow mixing, concentrating the walk in local neighbourhoods and repeating similar generators. This creates a correlation pathway with the focused/dispersed distinction (fast-mixing SCCs lean dispersed, slow-mixing lean focused), but the correlation is indirect and operates through the same gate-firing mechanism already captured by the firing count.

More importantly, γ is a purely topological quantity computed from P alone, independent of the WAR assignment W . It therefore cannot detect the WAR-dependent component of risk that DWS captures, and combining γ with DWS yields a two-variable Abelian composite more complex than the current baseline without guaranteed improvement. Fundamentally, γ is an eigenvalue of a commutative matrix operation and is therefore an Abelian statistic in the sense of Theorem 6.2: it provably cannot determine LE.

Cycle-count heuristics. It is tempting to count directed cycles [3] (or simple directed cycles of bounded length) in the SCC as a topological structure proxy: more cycles imply more opportunities for generator diversity and higher LE. However, cycle counts are purely topological and entirely blind to the WAR assignment. They are therefore *strictly more naive* than |DWS|, which integrates both topology (which edges are directed) and scalar (WAR values along those edges). Exact cycle enumeration is #P-hard in general; approximations add computational cost while providing less information than the Abelian baseline already in use. We do not consider cycle-count heuristics a competitive baseline.

WAR-weighted directed centrality. A more solid abelian alternative targets the *crossing-concentration* mechanism directly. For each node v , define its *ascending in-load*

$$\ell(v, W) = \sum_{\substack{(u \rightarrow v) \in E_{\text{dir}} \\ W(v) > W(u)}} (W(v) - W(u)),$$

so that $\text{DWS}(C, W) = \sum_v \ell(v, W)$. The *WAR-weighted centrality index* H measures how unevenly that load is distributed:

$$H(C, W) = \text{Gini}\left(\{\ell(v, W)\}_{v \in V}\right) = \frac{\sum_{v, u \in V} |\ell(v, W) - \ell(u, W)|}{2|V| \text{DWS}(C, W)},$$

with $H = 0$ for uniform load and $H = 1$ for a single-node hub. High H predicts focused behaviour; H is undefined when $\text{DWS} \leq 0$.

We tested H on all FD and DF disagreement samples from SCCs 216 and 207, classifying as focused when $H > 0.5$:

Error type	rate correct	H correct
FD: Bureau focused, rate false alarm (6 cases, SCC 216)	0/6	4/6
DF: Bureau dispersed, rate misses it (5 cases, SCC 207)	0/5	1/5
Total	0/11	5/11

Table 6: The centrality index: a local, specialized discriminator

H improves on the abelian rate for FD cases in SCC 216: ascending load concentrates on v_3 's strand, and the cases where $\text{DWS} > 0$ (cases with $\text{DWS} \in \{4, 5\}$) are correctly classified as

focused by $H > 0.5$. The four FD cases with $DWS < 0$ have undefined H and fall back to the default focused label.

However, this success is *structurally narrow*: H is valid only when (i) $DWS > 0$ (so that ℓ is well-defined and positive) and (ii) the topology is hub-shaped, routing ascending flow through a single dominant node. SCC 216 satisfies both conditions in the $DWS > 0$ subset; the broader 50 000-sample corpus shows that $DWS \leq 0$ in a majority of FD cases, making H inapplicable for most of them.

On DF cases H fails entirely (1/9): dispersed behaviour arises from generator diversity along the *paths feeding* the hub, a path-level ordering property that any node-aggregate discards by construction.

8.3 SCCs with the same primorial R

As discussed in [1], two SCCs in the same fusion class share the same R vector: same cycle count, same ordinal WAR relationships along each cycle edge. Within such a class, LE can still differ between instances: instances sharing the same ordinal structure may have different cardinal WAR magnitudes, placing them in different regimes. This is the precise sense in which the braid framework adds information that the primorial invariant cannot provide.

8.4 Limitations

- **Abelian rate cannot determine LE.** The gate-firing rate is an Abelian count of crossing events and cannot detect non-commutative cancellations. It provides a fast first-pass approximation that stabilises in half the epochs and walks required by Burau, but carries a systematic upward bias at the focused/dispersed boundary: it over-calls dispersed in all empirical disagreement cases. Temporal braid LE provides a practical non-Abelian proxy that corrects this bias, with partial correlation $r = 0.175$ with deployment structure versus $r = 0.001$ for counting LE.
- **The non-Abelian signal is small.** The shuffling experiment (Section 5.2) shows that the median gap between temporal log SR and shuffled log SR is only 1.3%. Temporal braid LE retains a partial correlation of $r = 0.175$ with deployment structure after controlling for firing rate; the non-commutative correction is statistically significant ($p < 10^{-3}$) but explains only 3% of the residual variance. Its value lies in providing a principled, theoretically grounded discrimination at the focused/dispersed boundary that Abelian statistics provably cannot achieve, even if the empirical magnitude of the correction is modest.
- **Small validation sample.** The 1,000-SCC corpus derives from a single synthetic generation procedure, and the classification’s robustness to real-world cloud IAM, Kubernetes RBAC, or enterprise Active Directory has not been established. The effectiveness of Burau LE as the focused/dispersed discriminator should therefore be understood as a working hypothesis confirmed within this corpus, not as a validated security primitive.
- **B_5 Burau representation is not faithful.** The Burau representation is unfaithful for B_n with $n \geq 5$ [7], so distinct braids in B_5 may map to the same matrix. Because our validation uses $n = 6$ walkers, this affects only the *validation* ground truth: non-faithfulness means distinct braids may share the same Burau matrix, so LE provides a lower bound on true braid complexity rather than an exact measure.

The operational impact is limited. Known kernel elements are long, highly structured words and are unlikely to arise from the short, randomized gate-injection words considered here. Moreover, non-faithfulness can only suppress spectral growth, yielding at worst conservative (downward-biased) Lyapunov estimates. Finally, the firing-rate lower bound

and the induced LE bound depend only on combinatorial firing rates and the exact per-injection spectral radius, both of which bypass the unfaithful $n \geq 5$ Burau kernel entirely.

9 Operability

The braid framework operates on SCCs already identified as *ratchets* by the primordial invariant; topological oscillators are filtered out before any dynamic analysis runs. Within ratchets, the two regimes are not merely classification labels: each implies a distinct mental model and a concrete intervention target. The critical operational boundary is between **focused** and **dispersed**: both require action but the action type is opposite.

Locating this boundary requires a non-Abelian instrument; Abelian statistics cannot determine LE (Theorem 6.2). *Bureau LE* defines the boundary and serves as the non-Abelian calibration oracle. The Abelian gate-firing rate is a useful conservative pre-filter (it over-calls dispersed, never under-calls) but cannot substitute for the non-Abelian screen at the boundary.

9.1 Regime-specific mental models

Focused (LE < 0.5847 for 6 vertices): the channelled ratchet. Escalation paths exist but traffic is concentrated through few directed edges. Non-commutative cancellations in the Bureau product moderate spectral growth, keeping LE below the dispersed threshold. The WAR assignment plays a key role: focused ratchets are WAR-sensitive, meaning that reassigning privileges to break the ascending alignment of directed edges will reduce LE and suppress the gate. The mental model is a funnel that can be blocked by removing the funnel’s gradient.

Dispersed (LE \geq 0.5847 for 6 vertices): the irreducible tangle. Hub-rich topology provides multiple independent escalation paths. Crossings accumulate without cancelling in the braid product, driving sustained high spectral growth. No WAR reassignment can suppress the gate because the hub topology sustains concurrent ascending traversals regardless of privilege alignment. The risk is in the graph structure itself. The mental model is an irreducible tangle: its complexity persists under any labelling.

9.2 Intervention summary

Regime	Mental model	Intervention target	Operator
focused	channelled ratchet	WAR assignment	reassign WAR
dispersed	irreducible tangle	edge set	add/remove edges

Table 7: Operability guide: mental model and intervention target per regime. Both regimes apply to ratchets (primordial-screened). The focused/dispersed boundary is defined by Bureau LE (impossibility separator, calibration oracle).

The intervention cost escalates monotonically: focused ratchets require an IAM-level privilege reassignment; dispersed ratchets require architectural-level changes to the permission graph, which may require review beyond standard IAM operations.

9.3 Complementarity with the primordial invariant

The primordial invariant and the braid framework answer different questions at different levels of the analysis pipeline:

- **Primorial (topology level): oscillators vs. ratchets.** The primorial invariant encodes the cycle structure of an SCC as a vector of rational numbers. Its output is a binary verdict: *oscillator* (topologically safe, no further analysis) or *ratchet* (escalation risk, proceed). Ratchets with identical escalation profiles are grouped into *fusion classes*, compressing the triage space.
- **Braid framework (deployment level): focused vs. dispersed.** Given a ratchet SCC and its ground-truth WAR assignment, the braid framework outputs LE, which determines whether the deployment is focused (WAR-remediable) or dispersed (topology-remediable). This determination is provably beyond Abelian statistics; only a non-Abelian instrument can supply it.

The two layers compose sequentially into a three-tier pipeline:

Primorial $\xrightarrow{\text{ratchet?}}$ Ratchet SCC $\xrightarrow{\text{temporal LE (non-Abelian screen) \text{ rate (fast triage) }}} \text{focused / dispersed} \rightarrow \text{Remediation.}$

Bureau LE sits *off the operational path*: it is not run in real-time screening.

Neither layer alone is sufficient. Primorial cannot assess deployed severity: the same ratchet topology can span both regimes depending on WAR assignment. Braids cannot replace the topological screen: running braid analysis on every SCC without primorial’s oscillator/ratchet filter would waste computation on structures incapable of escalation. Together they form a complete, two-layer risk pipeline with Bureau LE as the theoretical anchor.

10 Conclusion

No Abelian statistic can locate the boundary between focused and dispersed ratchets: Abelian measures are blind to edge-interleaving order, and therefore cannot detect the non-commutative cancellations that define the boundary (Theorem 6.2). This is not a quantitative gap to be closed by better counting; it is structural. Bureau LE is the separator that proves the gap and the calibration oracle that sets the threshold.

Empirically, across 49,972 (SCC, WAR) pairs from a 1000-SCC corpus, 5.7% of pairs disagree between Bureau and the Abelian rate, with a structured topology-dependent FD/DF pattern the rate cannot predict. Temporal braid LE retains partial correlation $r = 0.175$ with deployment structure after controlling for firing rate ($p < 10^{-3}$); counting LE collapses to $r = 0.001$ ($p = 0.98$).

The framework operates as a two-stage pipeline. The primorial invariant [1] screens SCCs as oscillators (safe) or ratchets (escalation-capable). Among ratchets, temporal braid LE provides the non-Abelian screen, partitioning deployments into the two regimes of Table 1 and directing each to its regime-appropriate intervention, with Bureau LE as the off-line calibration anchor.

10.1 Future work

Three directions extend the theoretical and practical reach of the framework.

Faithful representations. The Burau representation at $t = -1$ is unfaithful for $n \geq 5$ (Section 8), which limits the validation to a lower bound on braid complexity. The Lawrence–Krammer–Bigelow (LKB) representation [8] is faithful for all n . Replacing the Burau pipeline with LKB would eliminate the kernel issue entirely, at the cost of working with $\binom{n}{2} \times \binom{n}{2}$ matrices (15×15 at $n = 6$). A natural first step is to validate that the LE values produced by the LKB representation agree with the Burau values for the 82 ratchet topologies; any discrepancy would quantify the information lost to unfaithfulness and determine whether the $\approx 6 \times$ matrix-size increase is justified operationally.

Extending the firing-rate lower bound. The bound of Theorem 4.8 assumes a single high-privilege hub. Two natural generalisations remain open. (a) *Multi-hub topologies*: sum contributions of disjoint hub substructures separated by at least two rank positions (avoiding cross-cluster cancellation). (b) *Directed-cycle topologies*: Theorem 6.3 establishes that directed cycles have $\text{DWS}_{\text{cycle}} = 0$ for all WAR assignments, making them a class where Abelian screening is provably useless. The open problem is not the blindness (which is now proven) but a tighter *firing-rate lower bound*: SCCs whose directed edges form a cycle $v_1 \rightarrow \dots \rightarrow v_k \rightarrow v_1$ produce deterministic gate-firing patterns, and the resulting bounds should be tighter than the hub model, since walkers traverse ascending edges in a predictable rotation rather than via a random spoke-step. Both extensions could narrow the three-order-of-magnitude gap between the universal lower bound and observed LE in dense ratchets.

Injection word optimisation. The current framework fixes the injection word $\sigma_i^2 \sigma_{i+1}^{-1}$, selected for its spectral radius $2 + \sqrt{3}$ and its mixed-sign structure. The mixed sign is load-bearing: the negative exponent creates cross-epoch cancellations that Abelian statistics cannot detect, and this is precisely the mechanism behind the non-Abelian advantage ($r = 0.175$ partial correlation vs. $r = 0.001$ for counting LE).

One could ask whether sweeping the exponent pair (a, b) in $\sigma_i^a \sigma_{i+1}^b$ with $a > 0, b < 0$ could increase this marginal gain. Two effects pull in opposite directions. *Higher* $|b|$ deepens cross-epoch cancellations, potentially widening the gap between temporal and shuffled SR and amplifying the non-Abelian correction. *Higher* $|a|$ raises the per-firing SR contribution, increasing the raw LE signal but not necessarily the fraction of that signal invisible to Abelian counting.

References

- [1] C. Parisel. The primorial invariant. A Prime-Factorization Invariant for Classifying Cyclic Privilege Escalation in Cloud IAM. <http://dx.doi.org/10.2139/ssrn.6206079>, 2026.
- [2] E. Artin. Theory of braids. *Annals of Mathematics*, 48(1):101–126, 1947.
- [3] D. Johnson. Finding All the Elementary Circuits of a Directed Graph. *SIAM Journal on Computing, Volume 4, Issue 1*, 1975.
- [4] C. Parisel. Scoring Azure permissions with metric spaces. [arXiv:2504.13747](https://arxiv.org/abs/2504.13747), 2025.
- [5] R. Tarjan. Depth-first search and linear graph algorithms. *SIAM Journal on Computing*, 1(2):146–160, 1972.
- [6] J. S. Birman. *Braids, Links, and Mapping Class Groups*. Princeton University Press, 1974.
- [7] S. Bigelow. The Burau representation is not faithful for $n = 5$. *Geometry & Topology*, 3:397–404, 1999.
- [8] S. Bigelow. The Lawrence-Krammer representation. <https://arxiv.org/pdf/math/0204057>, 2002.
- [9] C. Parisel. Kaggle workbook with experimental results from this paper <https://www.kaggle.com/code/labyrinthinesecurity/braid-computing/>
- [10] J. Steele. Kingman’s subadditive ergodic theorem *Annales de l’I.H.P.*, section B, tome 25, 1989.
- [11] S. Khim. The Frobenius-Perron theorem <https://www.math.uchicago.edu/~may/VIGRE/VIGRE2007/REUPapers/FINALAPP/Khim.pdf>.

A Proofs for lower-bound growth rate

Proof of Theorem 4.6. Fix a walker i and an epoch $t \in \{1, \dots, T\}$.

Step 1: Spoke-step probability in terms of spoke-set occupation. Condition on the position of walker i at epoch t . If the walker is at vertex $v_j \in S$, it has at least one outgoing spoke edge ($v_j \rightarrow h$) and at most d_{\max} outgoing edges total, so the probability of choosing the spoke edge is at least $1/d_{\max}$. If the walker is at any vertex outside S , the probability of a spoke step is zero. Hence,

$$\mathbb{E}[X_{i,t}] \geq \frac{1}{d_{\max}} \sum_{j=1}^k \Pr(\text{walker } i \text{ is at } v_j \text{ at epoch } t).$$

Summing over all walkers and epochs and dividing by nT :

$$p_h \geq \frac{1}{d_{\max}} \sum_{j=1}^k \underbrace{\frac{1}{nT} \sum_{i=1}^n \sum_{t=1}^T \Pr(\text{walker } i \text{ is at } v_j \text{ at epoch } t)}_{=: \bar{\pi}(v_j)}.$$

Since C is strongly connected, the walk is irreducible with unique stationary distribution π . In stationarity $\bar{\pi}(v_j) = \pi(v_j)$; for arbitrary initialisation, $\bar{\pi}(v_j) \rightarrow \pi(v_j)$ as $T \rightarrow \infty$ by the ergodic theorem. It therefore suffices to lower-bound $\sum_j \pi(v_j)$, the total stationary mass on the spoke set.

Step 2a: Universal bound on $\pi(v_j)$ via path-chaining. Since $\sum_v \pi(v) = 1$, some vertex v^+ satisfies $\pi(v^+) \geq 1/|V|$. Because C is strongly connected, v^+ reaches any spoke vertex v_j via a directed path $x_0 = v^+ \rightarrow x_1 \rightarrow \dots \rightarrow x_\ell = v_j$ of length $\ell \leq \text{diam}(C)$. At each step, the stationary equation $\pi(w) = \sum_{u \rightarrow w} \pi(u)/d^+(u)$ implies $\pi(x_{m+1}) \geq \pi(x_m)/d_{\max}$ (the contribution from x_m alone, all other terms being non-negative). Iterating:

$$\pi(v_j) \geq \frac{1}{|V| \cdot d_{\max}^{\text{diam}(C)}}.$$

Substituting into Step 1:

$$p_h \geq \frac{k}{|V| \cdot d_{\max}^{\text{diam}(C)+1}}. \quad (\text{i})$$

Step 2b: Spoke-coverage bound via summed stationarity. The path-chaining argument bounds each $\pi(v_j)$ separately and discards all inflow to v_j except from one predecessor. When C is spoke-covered, we can instead bound $\sum_j \pi(v_j)$ *globally* by summing the stationary equations over the entire spoke set:

$$\sum_{j=1}^k \pi(v_j) = \sum_{j=1}^k \sum_{u: u \rightarrow v_j} \frac{\pi(u)}{d^+(u)} = \sum_{u \in V} \pi(u) \cdot \frac{|\{j : u \rightarrow v_j \in E\}|}{d^+(u)}.$$

If every vertex has out-edges to all k spoke vertices ($|\{j : u \rightarrow v_j\}| = k$ for all u) and $d^+(u) \leq d_{\max}$:

$$\sum_{j=1}^k \pi(v_j) \geq k \sum_{u \in V} \frac{\pi(u)}{d_{\max}} = \frac{k}{d_{\max}}.$$

Under the weaker spoke-coverage condition ($|\{j : u \rightarrow v_j\}| \geq 1$ for all u), the right-hand side is $1/d_{\max}$. Substituting the full-coverage case into Step 1:

$$p_h \geq \frac{1}{d_{\max}} \cdot \frac{k}{d_{\max}} = \frac{k}{d_{\max}^2}. \quad (\text{ii})$$

This bound is independent of $|V|$ and $\text{diam}(C)$: it avoids the path-chaining penalty entirely by using the full inflow to the spoke set from *every* vertex simultaneously.

Step 3: Concentration across walkers. Within a single walker, the indicators $X_{i,1}, \dots, X_{i,T}$ are Markov-dependent (the walker's position at epoch $t+1$ depends on its position at epoch t), so Hoeffding's inequality cannot be applied directly across epochs. However, the n walkers are *independent*.

Define the per-walker spoke-step frequency $Y_i = \frac{1}{T} \sum_{t=1}^T X_{i,t}$ for each walker $i = 1, \dots, n$. Each $Y_i \in [0, 1]$, and the Y_1, \dots, Y_n are independent (since the walkers perform independent random walks). The ensemble average is $\hat{p}_h = \frac{1}{n} \sum_{i=1}^n Y_i$. Applying Hoeffding's inequality to the n independent bounded random variables Y_1, \dots, Y_n :

$$\Pr[\hat{p}_h \leq \mathbb{E}[\hat{p}_h] - \epsilon] \leq \exp(-2n\epsilon^2).$$

The firing-rate theorem (Theorem 4.8) uses the *expected* firing count over T epochs: by linearity of expectation, $\mathbb{E}[M_T]$ is exact regardless of within-walker temporal dependence, so the lower bound requires no concentration assumption. The Hoeffding bound above provides an additional guarantee: as the number of walkers n grows, the empirical ensemble rate \hat{p}_h concentrates around its expectation, ensuring robustness against pathological individual walks. At the framework's $n = 6$, the concentration is modest; at larger n the bound tightens as $\exp(-\Omega(n))$. \square

Proof of Theorem 4.7. Let $A_i(t)$ be the indicator that walker i takes a spoke step at epoch t . Since the walkers perform independent random walks, $\Pr[A_i(t) \cap A_j(t)] = \Pr[A_i(t)] \cdot \Pr[A_j(t)] \geq p_h^2$ for every pair $i \neq j$. By linearity of expectation:

$$\mathbb{E}[m_{\text{spoke}}(t)] = \sum_{\{i,j\} \subseteq [n]} \Pr[A_i(t) \cap A_j(t)] \geq \binom{n}{2} p_h^2.$$

Substituting the bound from Theorem 4.6 gives the second inequality. \square

Proof of Theorem 4.8. Label walkers by NHI identifier $1 < 2 < \dots < n$ and fix the $\lfloor (n-1)/2 \rfloor$ non-overlapping pairs $\mathcal{P} = \{\{1, 2\}, \{3, 4\}, \dots\}$.

Each pair fires with probability $\geq p_h^2$. For $\{i, i+1\} \in \mathcal{P}$, the walkers are independent so $\Pr[A_i(t) \cap A_{i+1}(t)] \geq p_h^2$. When both fire, both traverse ascending spoke edges and both gate conditions (Theorem 3.2) are satisfied.

Hub-landing guarantees rank-adjacency. Every spoke edge terminates at h , so both walkers arrive at the same vertex with the same WAR value $W(h)$. Ties in WAR are broken by NHI identifier, placing the two walkers in consecutive ranks: the gate fires for this pair.

Non-overlapping pairs do not conflict. When multiple pairs in \mathcal{P} fire simultaneously, all hub-landing walkers are ordered by NHI index. The pairs $\{1, 2\}, \{3, 4\}, \dots$ occupy non-overlapping rank positions, so the adjacent-pair guard (Section 3.4) cannot block any pair in \mathcal{P} due to a firing by another.

Conclusion. The $\lfloor (n-1)/2 \rfloor$ firing events are independent (disjoint subsets of independent walkers) and each contributes probability $\geq p_h^2$. By linearity of expectation, summed over T epochs:

$$\mathbb{E}[M_T] \geq T \cdot \left\lfloor \frac{n-1}{2} \right\rfloor \cdot p_h^2. \quad \square$$

Proof of Theorem 4.9. Each gate firing multiplies the Burau product by the injection word's matrix, whose dominant eigenvalue is $2 + \sqrt{3}$ (Theorem 3.4). In the counting-LE model (which ignores cross-position spectral cancellation), M_T firings contribute $M_T \cdot \log(2 + \sqrt{3})$ to $\log \text{SR}(T)$. Dividing by T gives the per-epoch rate. The numerical bound follows from Theorem 4.8 with $p_h \geq k/(N \cdot d_{\max}^{D+1})$ from Theorem 4.6. \square